





Article

A Target to Combat Antibiotic Resistance: Biochemical and Biophysical Characterization of 3-Dehydroquinase Dehydratase from Methicillin-Resistant *Staphylococcus aureus*

Alfredo Téllez-Valencia ¹, Jesús Oria-Hernández ², Adriana Castillo-Villanueva ², Erick Sierra-Campos ³,
Mónica Valdez-Solana ³, Jorge Cisneros-Martínez ¹ and Claudia Avitia-Domínguez ^{1,*}

- ¹ Facultad de Medicina y Nutrición, Universidad Juárez del Estado de Durango, Av. Universidad y Fanny Anitua S/N, Durango 34000, Mexico; atellez@ujed.mx (A.T.-V.); jorgecisner10@yahoo.com.mx (J.C.-M.)
- ² Laboratorio de Bioquímica-Genética, Instituto Nacional de Pediatría, Insurgentes Sur 3700-C, Col. Insurgentes Cuicuilco, Alcaldía Coyoacán, Ciudad de Mexico 04530, Mexico; jesus.oria.inp@gmail.com (J.O.-H.); acastilloinp@gmail.com (A.C.-V.)
- ³ Facultad de Ciencias Químicas, Universidad Juárez del Estado de Durango Campus Gómez Palacio, Avenida Artículo 123 S/N, Fracc. Filadelfia, Gómez Palacio 35010, Mexico; ericksier@ujed.mx (E.S.-C.); valdezandyval@gmail.com (M.V.-S.)
- * Correspondence: claudia.avitia@ujed.mx

Abstract: Methicillin-resistant *Staphylococcus aureus* (MRSA) is associated with the acquisition of nosocomial infections, community-acquired infections, and infections related to livestock animals. In the pursuit of molecular targets in the development process of antibacterial drugs, enzymes within the shikimate pathway, such as 3-dehydroquinase dehydratase (DHQD), are regarded as promising targets. Therefore, through biochemical and biophysical techniques, in the present work, the characterization of DHQD from MRSA (*Sa*DHQD) was performed. The kinetic results showed that the enzyme had a V_{max} of 107 $\mu\text{mol}/\text{min}/\text{mg}$, a K_m of 54 μM , a k_{cat} of 48 s^{-1} , and a catalytic efficiency of 0.9 $\mu\text{M}^{-1} \text{s}^{-1}$. Within the biochemical parameters, the enzyme presented an optimal temperature of 55 °C and was thermostable at temperatures from 10 to 20 °C, being completely inactivated at 60 °C in 10 min. Furthermore, *Sa*DHQD showed an optimal pH of 8.0 and was inactivated at pH 4.0 and 12.0. Moreover, the activity of the enzyme was affected by the presence of ions, surfactants, and chelating agents. The thermodynamic data showed that the rate of inactivation of the enzyme was a temperature-dependent process. Furthermore, the enthalpy change, entropy change, and Gibbs free energy change of inactivation were positive and practically constant, which suggested that the inactivation of *Sa*DHQD by temperature was driven principally by enthalpic contributions. These results provide, for the first time, valuable information that contributes to the knowledge of this enzyme and will be useful in the search of *Sa*DHQD inhibitors that can serve as leads to design a new drug against MRSA to combat antibiotic resistance.

Keywords: MRSA; 3-dehydroquinase dehydratase; enzyme kinetics; biochemical characterization; thermodynamic parameters; antibiotic resistance



Citation: Téllez-Valencia, A.; Oria-Hernández, J.; Castillo-Villanueva, A.; Sierra-Campos, E.; Valdez-Solana, M.; Cisneros-Martínez, J.; Avitia-Domínguez, C. A Target to Combat Antibiotic Resistance: Biochemical and Biophysical Characterization of 3-Dehydroquinase Dehydratase from Methicillin-Resistant *Staphylococcus aureus*. *Microbiol. Res.* **2024**, *15*, 2316–2329. <https://doi.org/10.3390/microbiolres15040155>

Academic Editor:
Niels Frimodt-Møller

Received: 11 October 2024
Revised: 6 November 2024
Accepted: 9 November 2024
Published: 13 November 2024



Copyright: © 2024 by the authors. Licensee MDPI, Basel, Switzerland. This article is an open access article distributed under the terms and conditions of the Creative Commons Attribution (CC BY) license (<https://creativecommons.org/licenses/by/4.0/>).

1. Introduction

Growing antibiotic resistance with the increasingly frequent appearance of multidrug-resistant strains is mainly due to the uncontrolled and excessive use of antibiotics. Furthermore, the rapid exhaustion of new molecular targets after the so-called “the golden age of antibiotic discovery” have underscored the importance of seeking for and researching new antimicrobial drugs [1,2]. Furthermore, 4.95 million deaths worldwide were attributed to bacterial antibiotic resistance in 2019 [3]. In this context, the World Health Organization (WHO) issued a list of priority pathogens for the development and research of new drugs. One of these microorganisms was methicillin-resistant *Staphylococcus aureus* (MRSA),

classified as high priority [4], highlighting the necessity for research into new antibiotics against this bacterium [5]. In this context, the shikimate pathway (SHP), present in bacteria, archaea, plants, some protozoa, and fungi, whilst absent in humans, has been considered as promising molecular target to design new antimicrobial drugs [6]. This pathway includes seven reactions starting with the condensation of eritrose-4-P and phosphoenolpyruvate from the pentose phosphate and glycolysis routes, respectively, having chorismate as the final product. Chorismate is an intermediate in the synthesis of aromatic amino acids (tryptophan, phenylalanine, and tyrosine), folic acid, vitamin K, and ubiquinone, which supports the principal role of the enzymes in the SHP as potential drug targets [7]. The third reaction, the dehydration of 3-dehydroquinic acid to 3-dehydroshikimic acid, is catalyzed by 3-dehydroquinic acid dehydratase (DHQD), which exists as Type I and II isoforms (E.C. 4.2.1.10) [7]. Structurally, Type I DHQD is a thermolabile homodimer that only participates in the biosynthetic route. On the other hand, Type II is a thermostable homododecameric protein (four trimers) that can participate in the biosynthetic and in the catabolic pathways (shikimate and quinate, respectively) or in both, playing a dual role [7,8].

The relevance of DHQD as a viable molecular target is reinforced by investigations into *Shigella flexneri* strains that involved the deletion or inactivation of the *aroD* gene, which encodes for DHQD. The results showed that in monkeys vaccinated with these modified strains, the effectiveness against shigellosis ranged between 85 and 100% [9]. Furthermore, vaccines derived from *Francisella tularensis* strains with *aroD* gene deletion have a protective effect against tularemia in mice [10]. In the case of *S. aureus*, a study examined the growth of *S. aureus* strains with ochre mutations in the *aroD* gene. These strains were unable to grow in culture media without added aromatic amino acids [11]. Nowadays, only the crystallographic structure of DHQD from MRSA (*Sa*DHQD) is available; it belongs to the Type I DHQDs and is a homodimer with a TIM barrel fold in each monomer and a catalytic site at the center of the barrel [12]. This structure has a similar folding to those reported for *Salmonella typhi* [13], *Enterococcus faecalis* [14], and *Clostridium difficile* [15], which also belongs to the Type I DHQD group. Therefore, as a valuable target for antibiotic drug design, the aim of this study was to perform a biochemical and biophysical characterization of this enzyme to provide valuable information that can be used in the search of inhibitors to design a new antibiotic against MRSA.

2. Materials and Methods

2.1. *aroD* Gene Amplification, Cloning, and Overexpression

The amplification of the *aroD* gene encoding *Sa*DHQD was carried out by extracting genomic DNA from MRSA strain ATCC[®] BAA-1720 (Manassas, VA, USA) using the forward primer 5'-CCATATGACACATGTGGAAGTAGTAGCG-3' and the reverse primer 3'-CGGATCCTTAGTATAAAGTCACTTGTGC-5' with the *Nde*I and *Bam*HI restriction sites underlined. The amplification product was then cloned into the pJET1.2/Blunt vector (Thermo Scientific, Waltham, MA, USA) for sequence analysis. Thereafter, the gene was cloned into the pET-28a(+) vector (Novagen, Madison, WI, USA) and introduced by chemical transformation into *E. coli* BL21(DE3) (Novagen, Madison, WI, USA) cells for overexpression.

2.2. Protein Purification

*Sa*DHQD purification started from a 100 mL culture in LB broth media. The cells were allowed to grow at 37 °C and 200 rpm until an OD₆₀₀ nm of 0.9 AU. Thereafter, overexpression was induced by adding 1.0 mM IPTG and incubation at 37 °C and 200 rpm for three hours. Afterwards, cells were then harvested by centrifugation and washed with 50 mM Tris-HCl (pH 8.0). Next, the cells were resuspended in a lysis buffer (50 mM Tris-HCl pH 7.0, 500 mM NaCl, 10 mM β-mercaptoethanol (β-Met), and 0.03% v/v of Tween 20), adding 1 mM of the protease inhibitor phenylmethylsulfonyl fluoride (PMSF). The cell-free crude extract was recovered by centrifugation at 25,000 rpm at 4 °C for 30 min. *Sa*DHQD was purified by affinity chromatography, passing the cell-free crude extract through a

column packed with nickel–nitrilotriacetic acid (Ni-NTA) resin. Fractions were collected using a gradient of imidazole from 5 to 300 mM. The enzyme was eluted at a concentration of 100 mM imidazole. To remove imidazole, the fractions with the highest amount of *Sa*DHQD were pooled and washed with a buffer consisting of 50 mM Tris-HCl, 300 mM NaCl, and 10 mM β -Met at pH 8.0. The protein concentration was determined using the Bradford method [16].

2.3. Enzyme Activity

The enzymatic activity assays of *Sa*DHQD were performed using a modification of the method reported by Jaafar et al. [17]. The reaction mixture consisted of 50 mM Tris-HCl (pH 8.0), 200 μ M 3-dehydroquinic acid (3-DHQ), and 70 ng of *Sa*DHQD. The activity was measured spectrophotometrically at 25 °C by monitoring the production of 3-dehydroshikimic acid (3-DHS) ($\epsilon = 12,000 \text{ M}^{-1} \cdot \text{cm}^{-1}$) at 234 nm. One enzyme unit was defined as the amount of enzyme that catalyzes the conversion of 1 μ mole of substrate per minute under standard conditions. Experiments were conducted in triplicate for all determinations.

2.4. Biochemical Characterization

2.4.1. Amino Acid Sequence Analysis

To determine similarities at the sequence level, a multiple sequence alignment of *Sa*DHQD and other Type I DHQDs from bacteria was performed using Clustal W [18] and the Easy Sequencing in PostScript program (ESPrpt3.0) [19].

2.4.2. Kinetic Parameters

To determine the kinetic parameters (K_m and V_{max}), curves were generated using the reaction mixture described above with varying concentrations of 3-DHQ ranging from 5 to 500 μ M. K_m and V_{max} values were calculated fitting the data to Michaelis–Menten equation using SigmaPlot V15.0 software. On the other hand, the k_{cat} and catalytic efficiency (k_{cat}/K_m) values were obtained applying the equations reported earlier [20].

2.4.3. Optimum pH

Enzyme optimum pH determination was carried out using a modification of the method reported by Avitia-Domínguez et al. [21], measuring enzymatic activity under the conditions described above at different pH values. To this end, the following buffers were used: 0.1 M citric acid–0.2 M Na_2HPO_4 (pH 4.0 to 6.0) and 0.05 M Tris-HCl (pH 7.0 to 9.0); 0.05 M NaHCO_3 –0.1 M NaOH (pH 10.0 and 11.0); and 0.2 M KCl–0.2 M NaOH (pH 12.0). Optimum pH was defined as the pH at which the highest enzymatic activity was obtained, taking this value as 100% to calculate the relative activity at the other pH values.

2.4.4. pH Stability

The stability of *Sa*DHQD was obtained by incubating the enzyme at a pH range from 4.0 to 12.0 using the previously mentioned buffers, over a time interval from 0 to 240 h. The initial activity at each pH was taken as 100% to calculate the residual activity over the time.

2.4.5. Optimum Temperature

To determine the optimal temperature, enzymatic activity was measured in a range from 10 to 60 °C. Optimum temperature was defined as the temperature at which the highest enzymatic activity was obtained, taking this value as 100% to calculate the relative activity at the other temperature values.

2.4.6. Thermal Stability

To assess the thermal stability, the enzyme was incubated in a range from 10 to 60 °C over a time interval from 0 to 72 h. The initial activity at each temperature was taken as 100% to calculate the residual activity over the time.

2.4.7. Effect of Ions, Surfactants, and Chelating Agents

To understand the impact of ions, surfactants, and chelating agents on the activity of *Sa*DHQD, the effect of ions such as Na⁺, K⁺, NH₄⁺, Ca²⁺, Mg²⁺, Ba²⁺, Mn²⁺, and Fe³⁺; surfactants such as sodium dodecyl sulfate (SDS), Triton X-100, and Tween 20; and the chelating agent ethylenediaminetetraacetic acid (EDTA) at 1 and 5 mM was measured. Activity under standard conditions was taken as 100% to calculate the relative activity in each case. The statistical significance of the data was analyzed by Welch's *t*-test.

2.4.8. Structural Characterization

The secondary structure was evaluated by circular dichroism (CD) in the far-UV region (190–280 nm) in a Jasco J-810 spectropolarimeter (Ishikawamachi Hachioji-shi, Tokyo, Japan). Assays were performed at 25 °C and a protein concentration of 0.1 mg/mL in a 50 mM phosphate buffer at pH 7.4. The tertiary structure was assessed by intrinsic protein fluorescence (300–500 nm) in a Perkin-Elmer LS-55 fluorescence spectrometer (Waltham, MA, USA) after excitation at 280 nm. Assays were conducted at 25 °C in a 50 mM phosphate buffer (pH 7.4) and a protein concentration of 0.1 mg/mL. The quaternary structure was evaluated by size exclusion chromatography in a Superose 6 10/300 GL column (GE Healthcare, Chicago, IL, USA) coupled to an Äkta FPLC system (GE Healthcare, Chicago, IL, USA), previously calibrated with molecular mass standards; the running conditions were 25 °C and 50 mM Tris–HCl (pH 8.0) plus 150 mM NaCl. Protein stability was investigated by following the CD signal at 222 nm in response to temperature scans from 25 to 90 °C (1 °C/min); the protein concentration was 0.1 mg/mL in a 50 mM phosphate buffer at pH 7.4. The unfolding protein fraction and melting temperature were calculated as reported [22]. In the spectroscopic assays, the blank spectra were subtracted from experimental ones.

2.5. Thermodynamic Parameters

Based on the data obtained from the optimum temperature and thermal stability assays, the values for activation and inactivation energy, enthalpy, entropy, and Gibbs free energy change were determined.

2.5.1. Activation Energy

The activation energy (E_a , kJ mol⁻¹) was calculated from optimum temperature experiments using a modification of the Arrhenius equation (Equation (1)), where R is the ideal gas constant (8.314462 J K⁻¹ mol⁻¹), A is the Arrhenius constant, T (K) is the absolute temperature, and v (μmol min⁻¹ mg⁻¹) is the enzyme activity at temperature T in the range where its value was increasing. The value of E_a was obtained from the slope of the plot according to Equation (2).

$$\ln(v) = \left(-\frac{E_a}{R}\right)\frac{1}{T} + \ln(A) \quad (1)$$

$$\text{slope} = \frac{E_a}{R} \quad (2)$$

2.5.2. Thermal Inactivation Parameters

From the thermal stability assays, inactivation rate constants at a specific temperature (k_d , h⁻¹) were calculated using Equation (3), where A_0 and A_i represent the initial and residual enzyme activity, respectively, and t is the incubation time. The rate constants obtained were used in Equation (4) to calculate the activation energy of denaturation or inactivation energy (E_d) based on the Arrhenius equation. The E_d value was obtained from the slope of the plot as in Equation (2).

$$\ln\left(\frac{A_i}{A_0} \cdot 100\right) = (-k_d)t \quad (3)$$

$$\ln(k_d) = \left(-\frac{E_d}{R}\right)\frac{1}{T} + \ln(A) \quad (4)$$

Furthermore, the time necessary for the enzyme to lose 50% of its activity (the half-life ($t_{1/2}$)) and the time to lose 90% (the decimal reduction time (D-value)) [23] were also calculated at each specific temperature using Equations (5) and (6).

$$t_{1/2} = \frac{\ln(2)}{k_d} \quad (5)$$

$$D = \frac{\ln(10)}{k_d} \quad (6)$$

The enthalpy (ΔH), Gibbs free energy (ΔG), and the entropy (ΔS) variation at each temperature were calculated using Equations (7), (8), and (9), respectively, using the previously obtained k_d values, where h is the Planck constant (6.6262×10^{-34} J s) and K is the Boltzmann constant (1.380649×10^{-23} J K⁻¹).

$$\Delta H = E_d - RT \quad (7)$$

$$\Delta G = -RT \ln\left(\frac{k_d h}{KT}\right) \quad (8)$$

$$\Delta S = \frac{\Delta H - \Delta G}{T} \quad (9)$$

3. Results and Discussion

3.1. Biochemical Characterization

3.1.1. Sequence Analysis of SaDHQD

SaDHQD consisted of 714 nucleotides encoding 238 amino acid residues. Sequence alignment with other Type I dehydroquinases from *Escherichia coli*, *Salmonella typhi*, *Bacillus subtilis*, *Klebsiella pneumoniae*, *Acinetobacter baumannii*, *Streptococcus pyogenes*, and *Streptococcus pneumoniae* (Figure 1) showed that SaDHQD contains all the conserved residues (Glu35, Arg37, Arg70, Lys160, His133, Arg202, and Gln225), which are crucial for catalysis [15,24] (Figure 2). Furthermore, according to the alignment, the identity percentage in comparison with the other DHQDs was 30% for *E. coli*, 35% for *S. typhi* and *B. subtilis*, 31% for *K. pneumoniae*, 32% for *A. baumannii*, and 29% for *S. pyogenes* and *S. pneumoniae*. The percentage of similarity ranged from 50 to 55%, suggesting that, although no structural data are available, except for *E. coli* and *S. typhi*, all of them will show the same TIM barrel folding.

3.1.2. Purification of SaDHQD

The enzyme underwent one-step purification via affinity chromatography (Table 1) resulting in a sevenfold enrichment with 40% recovery of the enzyme. SDS-PAGE of the purified enzyme (Figure 3A) showed only one band with a molecular weight consistent with the predicted from the sequence analysis (~27 kDa). Size exclusion chromatography (Figure 3B) indicated that, as was reported for the crystallographic structure [12], the native state of the protein is a dimer, as inferred from the molecular mass of 57.5 kDa calculated from the elution time. These data closely resemble the mass calculated from the amino acid sequence; the difference can be explained by the His-tag and the additional amino acids incorporated during gene cloning into the expression plasmid. Furthermore, this oligomeric state is like that reported for other Type I DHQDs in bacteria [13].

Table 1. Summary of the purification process of SaDHQD.

	Volume (mL)	Protein (mg)	Total Activity (U)	Specific Activity (U/mg)	Purification (Fold)	Yield (%)
Crude extract	20	18.59	124.28	6.68	1.00	100.00
Affinity chromatography	3	1.02	50.20	49.34	7.48	40.4

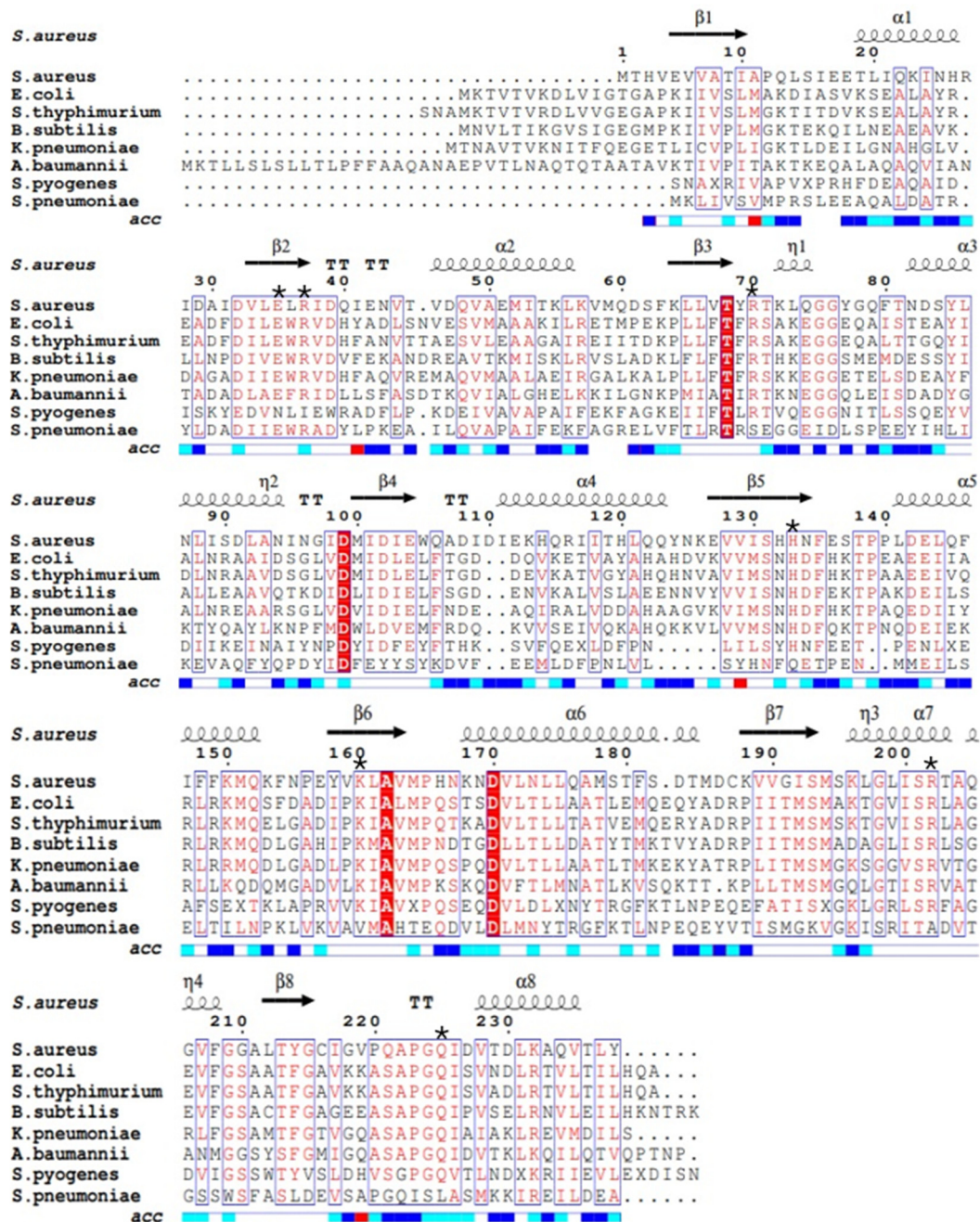


Figure 1. Sequence alignment of SaDHQD with Type I DHQD from *E. coli*, *S. typhi*, *B. subtilis*, *K. pneumoniae*, *A. baumannii*, *S. pyogenes*, and *S. pneumoniae*. Conserved residues (red text) are indicated in purple boxes and highly conserved residues in red boxes. The secondary structure is indicated at the top of the sequence alignment; the β sheets are represented as arrows and the α -helix as spirals, and the TT indicates turns. The colored boxes at the bottom of the residues indicate their accessibility to the solvent, where blue represents accessible, cyan represents intermediate accessibility, white represents poor accessibility, and red represents non-calculable accessibility. The active site's residues are indicated with an asterisk.

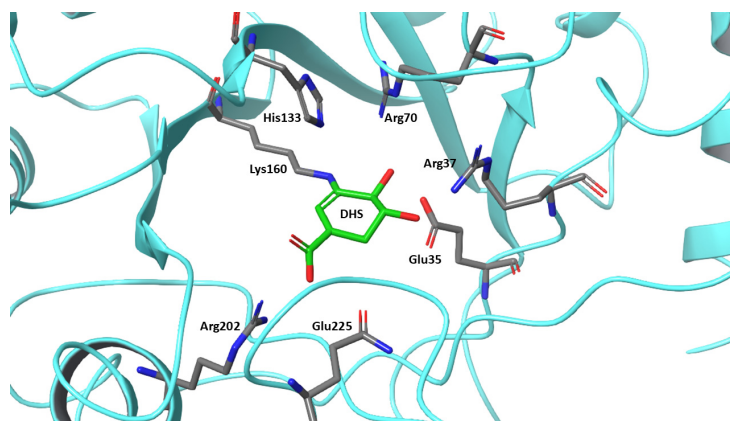


Figure 2. Close-up view of the catalytic site from *Sa*DHQD in complex with 3-dehydroshikimate (DHS), showing the adduct formed with Lys160 before product release. The image was generated on the basis of the crystallographic structure from *Sa*DHQD reported in [12].

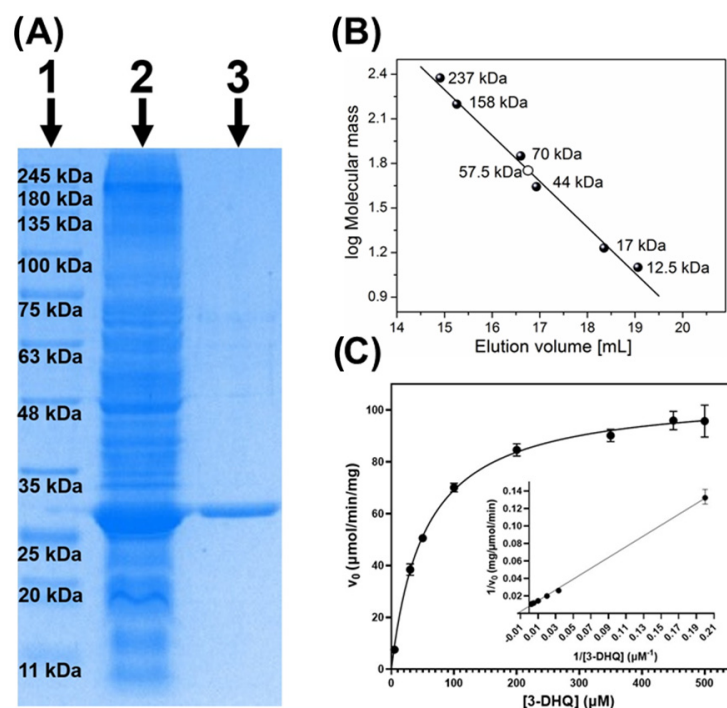


Figure 3. Purification and kinetic characterization of *Sa*DHQD. (A) SDS-PAGE analysis for the purification process: Lane 1, molecular weight marker; Lane 2, crude extract; Lane 3, purified *Sa*DHQD. (B) Size exclusion chromatography calibration curve to determine the molecular weight of *Sa*DHQD in native conditions. (C) The Michaelis–Menten kinetics curve for *Sa*DHQD; the inset shows the Lineweaver–Burk plot.

3.1.3. Kinetic Characterization of *Sa*DHQD

The enzyme showed a hyperbolic kinetic behavior (Figure 3C) like its counterparts in other bacteria [25–27]. The kinetic parameters obtained were a K_m of 54 μM , a V_{\max} of 107.7 $\mu\text{mole}/\text{min}/\text{mg}$, a k_{cat} of 48.5 s^{-1} , and a catalytic efficiency of 0.9 $\mu\text{M}^{-1} \text{s}^{-1}$. These values were like those reported for homologous enzymes in *Enterococcus faecalis* [14] and *Clostridium difficile* [15].

3.1.4. Effect of pH and Temperature on *Sa*DHQD Activity

Assays at different pH showed that the optimum pH for *Sa*DHQD was 8.0 (Figure 4A), which is equal to that reported for DHQDs from *Escherichia coli* [28] and *Gluconobacter*

oxydans [29], despite belonging to different families (Enterobacteriaceae for *E. coli* and Acetobacteraceae for *G. oxydans*).

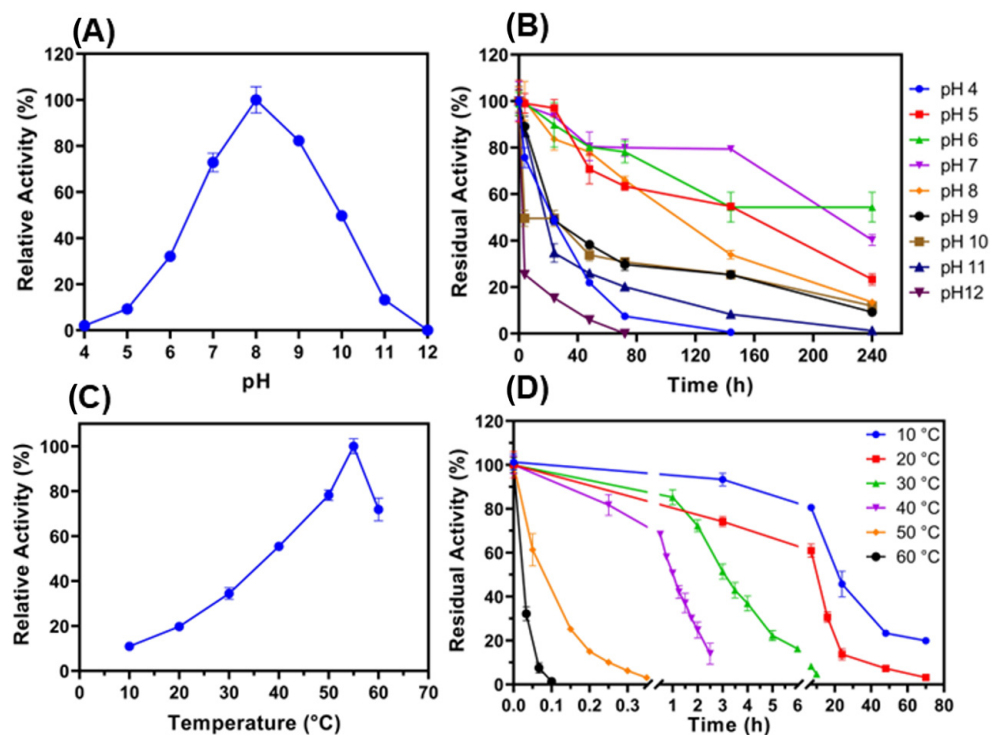


Figure 4. Effect of pH and temperature on the relative activity (%) of SaDHQD. (A) Optimum pH. (B) pH stability. (C) Optimum temperature. (D) Thermostability.

In the case of the protein stability at varying pH, the enzyme retained its activity for a longer time at pH 6.0 and 7.0, with 54.4% and 40.26% residual activity after an incubation of 240 h, respectively. On the other hand, at pH 4.0 and 12.0, the enzyme lost its activity after 144 h and 72 h, respectively (Figure 4B).

In respect to the effect of temperature on SaDHQD's activity, the results indicated that its optimum temperature was 55 °C; at higher values, the activity began to decrease (Figure 4C). Furthermore, the enzyme exhibited a thermolabile character by being completely inactivated at 60 °C after 10 min (Figure 4D), like that reported for its counterpart Type I DHQD from *G. oxydans*, which was inactivated at 70 °C in 10 min [29]. In contrast, as mentioned before, Type II DHQDs are thermostable, such as that from *S. coelicolor*, which, at 80 °C for 80 min, did not lose activity or that from *G. oxydans* (Type II, this bacterium has both isoforms), which only lost 10% of its activity at 70 °C for 10 min [29].

3.1.5. Effect of Metal Ions and Surfactants on SaDHQD's Activity

As a part of biochemical characterization, it was interesting to test the effect of different ions and other chemical agents (surfactant and chelating molecules) on SaDHQD's activity (Figure 5A). At a concentration of 1 mM, ions such as Ca²⁺, Mg²⁺, and Fe³⁺ exhibit slightly activating effects, showing relative activities of 120%, 111%, and 110%, respectively. However, the enzyme activity decreases by 40% at the same concentration with Mn²⁺ ions. On the contrary, ions such as Na⁺, K⁺, NH₄⁺, Mg²⁺, and Ba²⁺ did not cause a decrease in enzyme activity greater than 10% even at the highest concentration (5 mM). On the other hand, some surfactants, such as SDS and Triton X-100, reduced the enzyme activity by 78 and 100% at a concentration of 1 mM, respectively. However, Tween 20 only diminished the activity by around 35% at 5 mM. For the chelating agent, EDTA, it inhibited the activity by 86% at 5 mM. It is important to mention that all these differences were statistically significant (Table 2). The data suggest that even though the enzyme is not a metalloenzyme,

its structure can still be altered by the binding of certain ions and a chelating agent [14,28]. Therefore, these potential binding sites could be used as a starting point to design inhibitors for *Sa*DHQD.

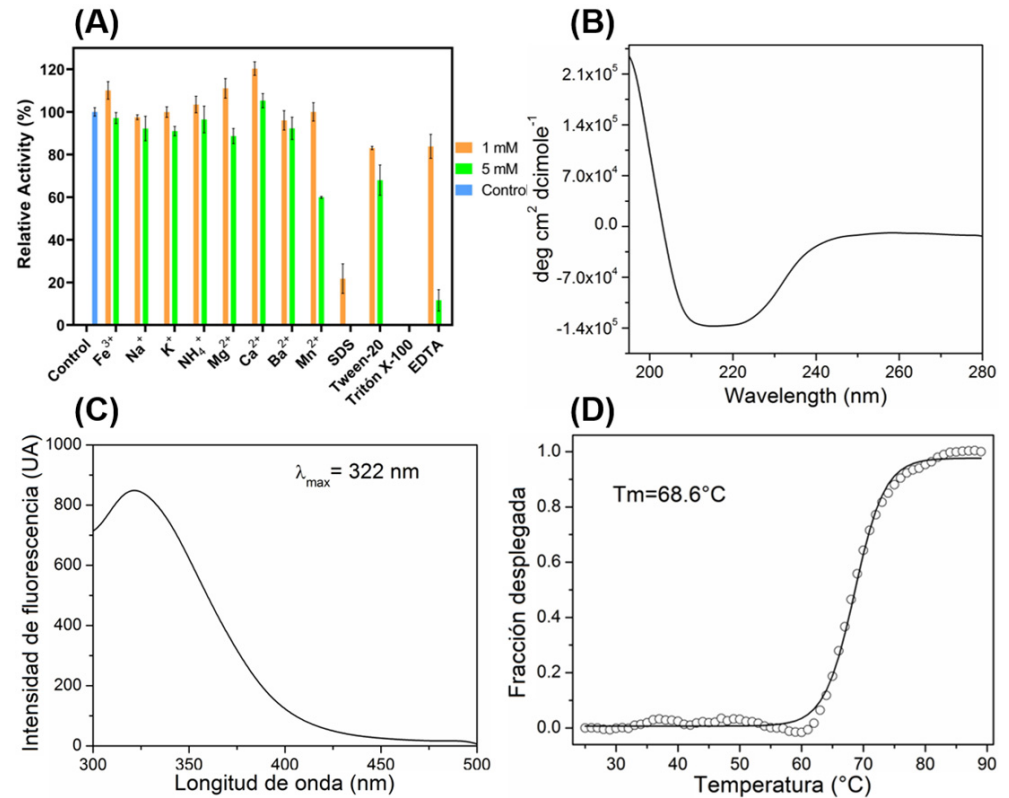


Figure 5. Effect of different agents on *Sa*DHQD's activity and structural analysis. (A) Effect of metal ions and surfactants on *Sa*DHQD's activity. (B) Far-UV circular dichroism spectrum of *Sa*DHQD. (C) Fluorescence spectrum of *Sa*DHQD. (D) Thermal denaturation of *Sa*DHQD.

Table 2. Statistical analysis of the effect of ions, surfactants, and chelating agents on the activity of *Sa*DHQD.

Ions, Surfactants, and Chelating Agents	<i>p</i> * Value at Different Concentrations	
	1 mM	5 mM
Na ⁺	0.1448	0.1342
K ⁺	0.9699	0.0064
NH ₄ ⁺	0.2623	0.4330
Mg ²⁺	0.0380	0.0152
Ca ²⁺	0.0016	0.0940
Ba ²⁺	0.2657	0.116
Mn ²⁺	0.9932	0.0005
Fe ³⁺	0.0343	0.2048
SDS	0.0014	0.0001
Tween-20	0.0018	0.0115
Tritón-X-100	0.0001	0.0001
EDTA	0.0273	0.0002

* *p* value ≤ 0.05 indicates statistical significance.

3.1.6. Circular Dichroism and Fluorescence Analysis

The circular far-UV dichroism spectra of *Sa*DHQP showed a minimum between 221 and 212 nm (Figure 5B), indicative of an α/β protein, which agrees with the TIM barrel structure determined by protein crystallography [12]. The CD spectrum of *Sa*DHQP resembles those of *E. coli* [30] and *S. typhi* [26] and agrees with the TIM barrel three-dimensional structure of Type I DHQDs [12,13]. On the other hand, the protein fluorescence spectrum showed the maximum fluorescence intensity at 322 nm after excitation at 280 nm (Figure 5C). The fluorescence maximum emission at 322 nm indicated that fluorophores are buried in non-polar environments of the protein (Tyr15, Tyr69, Tyr77, Tyr85, Tyr124, Tyr158, Tyr214, Tyr238, and Trp105). According to the results observed in the crystal structure [12], only Tyr15, Tyr77, and Tyr124 are exposed to solvent, suggesting that these residues practically do not contribute to the fluorescence detected. Finally, the thermal stability of *Sa*DHQP was evaluated, following the CD signal as a function of temperature (Figure 5D); from these data, a T_m of 68.6 °C was obtained. This value is higher compared with the T_m reported for DHQDs from *S. typhi* (55.5 °C) [26] and from *E. coli* (57.2 °C) [30]. The result is concordant with the comparative analysis of these proteins, which showed that *Sa*DHQP is a more compact dimer with higher structural rigidity [12].

3.2. Thermodynamic Parameters

Kinetic stability is defined as the resistance of an enzyme to irreversible inactivation. Moreover, thermodynamic stability is defined as the difference in free energy between the native and unfolded states of an enzyme [31]. This information is relevant in the characterization of a potential drug target. Therefore, the kinetic stability and thermodynamic parameters for thermal inactivation of *Sa*DHQP were determined (Table 3). Firstly, the activation energy E_a , referred as the energy necessary for the conversion of the substrate to the product, was estimated from the enzyme activity in the range where the velocity increased with temperature (Figure 4C), applying the Arrhenius plot (Figure 6A). As far as we know, there are not reports about E_a for other DHQDs from bacteria; therefore, it is not possible to state if the value obtained for *Sa*DHQP is higher or lower. However, it has been reported that a higher value of E_a makes the profile in the temperature curve become sharper [32,33]. According to the results observed in *Sa*DHQP, a 5-degree change in temperature (55 to 60 °C) causes a dramatic loss in activity (Figure 4C). Therefore, this behavior suggests that *Sa*DHQP has a higher energy of activation. Furthermore, this value also depends on the purity of the enzyme's preparation; a crude extract showed a higher value with respect to the pure enzyme [31]. In the case of *Sa*DHQP, according to the purity of the enzyme, it can be stated that the value obtained was not overestimated. Finally, a higher E_a suggests that the active site is less favorable for substrate binding, causing a lower catalytic efficiency [34,35]. Unfortunately, we are without other values to compare this with, so maybe this could be the case for *Sa*DHQP.

Continuing with thermodynamic characterization, other parameters, such as the inactivation constant (k_d), the enzyme's half-life ($t_{1/2}$), and the decimal reduction time (D-value), were determined at different temperatures (Table 3). From these data, the energy necessary to start enzyme inactivation (E_d) was determined on the basis of applying k_d values, as in the case of E_a , with the Arrhenius plot obtaining a value of 126.6 kJ/mol (Figure 6B). A higher E_d value implies higher enzyme stability; however, as no values are reported for other DHQDs, there is no way to know if the E_d from *Sa*DHQP is lower or higher, but it will be helpful as a starting point for comparison in future determinations with homologous enzymes. Moreover, the linearity of the plot suggests that the inactivation of the enzyme is a process that is dependent on the temperature [36]. Because this value alone is not sufficient to evaluate enzyme thermal stability, additional thermodynamic parameters were determined.

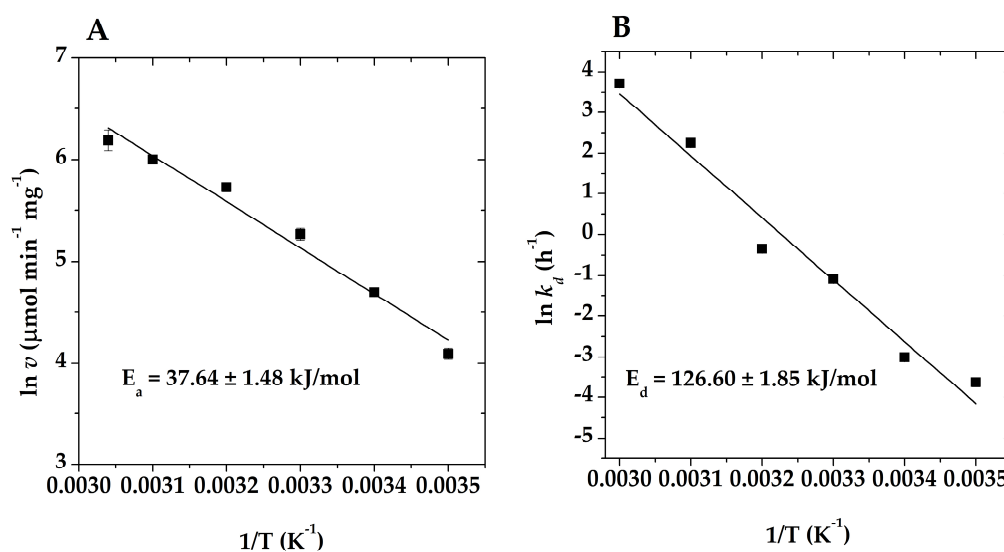


Figure 6. Arrhenius plots to determine the activation (A) and inactivation (B) energies of *SaDHQD*.

Table 3. Kinetic stability and thermodynamic parameters of *SaDHQD*.

Temperature (K)	k_d (h ⁻¹)	$t_{1/2}$ (h)	D (h)	ΔH (kJ/mol)	ΔG (kJ/mol)	ΔS (kJ/mol K)
283.15	0.026 ± 0.003	26.66	88.56	124.25	97.10	0.096
293.15	0.050 ± 0.002	13.86	46.05	124.16	99.05	0.086
303.15	0.333 ± 0.011	2.06	6.92	124.08	97.70	0.087
313.15	0.704 ± 0.027	0.985	3.27	123.99	99.07	0.080
323.15	9.533 ± 0.180	0.073	0.24	123.91	95.31	0.088
333.15	41.72 ± 1.291	0.017	0.055	123.83	94.25	0.089

One of them was the enthalpy change (ΔH), a parameter related with the non-covalent bonds broken during enzyme inactivation [37]. The data showed that this value did not suffer important variations in the range of temperatures assessed (Table 3). This behavior suggests that the enzyme inactivation was driven principally by the structural changes due to temperature increases. Furthermore, the dramatic inactivation observed at temperatures beyond 40 °C supports the principal role of enthalpic contributions in accelerating the breakage of non-covalent interactions, which causes the inactivation of the enzyme [36]. In the same context, the determination of the entropy change (ΔS), related to disordering of the enzyme and solvent [37], showed that this value was positive and constant along the temperature range (Table 3). However, in comparison with ΔH , this value was close to zero, which indicates an increase in the disorder in the protein/solvent system upon enzyme inactivation [37]. Additionally, this behavior reinforces the importance of enthalpic contributions, suggesting that the rate-limiting step for enzyme inactivation was protein unfolding [38]. On the contrary, it had a negative ΔS value, which maybe means that the inactivation could be due to the aggregation of partially unfolded protein [39]. Finally, the Gibbs free energy change (ΔG) that involves the energy barrier for enzyme inactivation [37] had a practically constant value (Table 3). The abovementioned findings suggest that there exists a decrease in the enzyme's susceptibility to inactivation as the temperature increase [36]. Further studies with homologous enzymes are needed to compare the thermodynamic parameters described here for *SaDHQD*.

3.3. Design of Potential Inhibitors

In the search for or design of new inhibitors from an enzyme of interest, all available information is valuable; the structural, kinetic, and thermodynamic parameters of the enzyme are important. The data reported in this work showed that *SaDHQD* can bind some ions as well as chelating agents, and that the binding of some of these provokes the

inhibition of the enzyme. Furthermore, the alignment and the structural data of homologous DHQDs, which are very similar in all of them, suggest that a potential inhibitor with an effect on the DHQDs from different bacteria could be designed with these binding sites as the target, or they could also be directed to the active site that is highly conserved, taking advantage of how this enzyme is absent in humans. In this context, only irreversible inhibitors that bound covalently to Lys160 have been reported for *Sa*DHQD and *S. typhi* DHQDs [40,41]. Furthermore, a computational study reported the first non-covalent potential inhibitors from *Sa*DHQD with the catalytic site as a target [42].

Therefore, the data reported here encourage further studies to search for or design new DHQD inhibitors.

4. Conclusions

To the best of our knowledge, this is the first study about the biochemical and thermodynamic characterization of *Sa*DHQD. These results provide valuable information that contributes to the knowledge of this enzyme and will be useful in the search for and design of *Sa*DHQD inhibitors that can serve as leads to design a new drug against MRSA to combat antibiotic resistance.

Author Contributions: Conceptualization, A.T.-V. and C.A.-D.; methodology, E.S.-C., M.V.-S., J.O.-H., A.C.-V., A.T.-V. and C.A.-D.; formal analysis, E.S.-C., M.V.-S., J.O.-H., A.C.-V., J.C.-M., A.T.-V. and C.A.-D.; writing—original draft preparation, A.T.-V. and C.A.-D.; writing—review and editing, E.S.-C., M.V.-S., J.O.-H., A.C.-V., A.T.-V. and C.A.-D.; funding acquisition, C.A.-D. All authors have read and agreed to the published version of the manuscript.

Funding: This research was funded by Consejo Nacional de Humanidades Ciencias y Tecnologías (CONAHCyT), grant number CF-2023-I-2312, to C.A.-D.

Institutional Review Board Statement: Not applicable.

Informed Consent Statement: Not applicable.

Data Availability Statement: Data are contained within the article.

Acknowledgments: The authors thank Fabián Corral-Rodríguez for technical assistance.

Conflicts of Interest: The authors declare no conflicts of interest.

References

1. Fernandes, P.; Martens, E. Antibiotics in late clinical development. *Biochem. Pharmacol.* **2017**, *133*, 152–163. [CrossRef] [PubMed]
2. Hutchings, M.; Truman, A.; Wilkinson, B. Antibiotics: Past, present and future. *Curr. Opin. Microbiol.* **2019**, *51*, 72–80. [CrossRef] [PubMed]
3. Murray, C.J.L.; Ikuta, K.S.; Sharara, F.; Swetschinski, L.; Aguilar, G.R.; Gray, A.; Han, C.; Bisignano, C.; Rao, P.; Wool, E.; et al. Global burden of bacterial antimicrobial resistance in 2019: A systematic analysis. *The Lancet* **2022**, *399*, 629–655. [CrossRef] [PubMed]
4. WHO Bacterial Priority Pathogens List. Bacterial Pathogens of Public Health Importance to Guide Research, Development and Strategies to Prevent and Control Antimicrobial Resistance. 2024. Available online: <https://www.who.int/publications/i/item/9789240093461> (accessed on 1 November 2024).
5. Mahjabeen, F.; Saha, U.; Mostafa, M.N.; Siddique, F.; Ahsan, E.; Fathma, S.; Tasnim, A.; Rahman, T.; Faruq, R.; Sakibuzzaman, M.; et al. An Update on Treatment Options for Methicillin-Resistant Staphylococcus aureus (MRSA) Bacteremia: A Systematic Review. *Cureus* **2022**, *14*, e31486. [CrossRef] [PubMed]
6. Frlan, R. An Evolutionary Conservation and Druggability Analysis of Enzymes Belonging to the Bacterial Shikimate Pathway. *Antibiotics* **2022**, *11*, 675. [CrossRef]
7. Mir, R.; Jallu, S.; Singh, T.P. The shikimate pathway: Review of amino acid sequence, function and three-dimensional structures of the enzymes. *Crit. Rev. Microbiol.* **2015**, *41*, 172–189. [CrossRef]
8. Nunes, J.E.S.; Duque, M.A.; de Freitas, T.F.; Galina, L.; Timmers, L.F.S.M.; Bizarro, C.V.; Machado, P.; Basso, L.A.; Ducati, R.G. Mycobacterium tuberculosis shikimate pathway enzymes as targets for the rational design of anti-tuberculosis drugs. *Molecules* **2020**, *25*, 1259. [CrossRef]
9. Jennison, A.V.; Verma, N.K. Shigella flexneri infection: Pathogenesis and vaccine development. *FEMS Microbiol. Rev.* **2004**, *28*, 43–58. [CrossRef]

10. Cunningham, A.L.; Mann, B.J.; Qin, A.; Santiago, A.E.; Grassel, C.; Lipsky, M.; Vogel, S.N.; Barry, E.M. Characterization of Schu S4 aro mutants as live attenuated tularemia vaccine candidates. *Virulence* **2020**, *11*, 283–294. [[CrossRef](#)]
11. Zhang, P.; Wright, J.A.; Osman, A.A.; Nair, S.P. An aroD Ochre mutation results in a Staphylococcus aureus Small colony variant that can undergo phenotypic switching via two alternative mechanisms. *Front. Microbiol.* **2017**, *8*, 1001. [[CrossRef](#)]
12. Nichols, C.E.; Lockyer, M.; Hawkins, A.R.; Stammers, D.K. Crystal structures of Staphylococcus aureus type I dehydroquinase from enzyme turnover experiments. *Proteins Struct. Funct. Bioinform.* **2004**, *56*, 625–628. [[CrossRef](#)] [[PubMed](#)]
13. Coggins, J.R.; Sawyer, L.; Gourley, D.G.; Shrive, A.K.; Polikarpov, I.; Krell, T.; Hawkins, A.R.; Isaacs, N.W. The two types of 3-dehydroquinase have distinct structures but catalyze the same overall reaction. *Nat. Struct. Mol. Biol.* **1999**, *6*, 521–525. [[CrossRef](#)] [[PubMed](#)]
14. Cheung, V.W.N.; Xue, B.; Hernandez-Valladares, M.; Go, M.K.; Tung, A.; Aguda, A.H.; Robinson, R.C.; Yew, W.S. Identification of polyketide inhibitors targeting 3-dehydroquinase dehydratase in the shikimate pathway of Enterococcus faecalis. *PLoS ONE* **2014**, *9*, e103598. [[CrossRef](#)] [[PubMed](#)]
15. Light, S.H.; Minasov, G.; Shuvalova, L.; Duban, M.-E.; Caffrey, M.; Anderson, W.F.; Lavie, A. Insights into the mechanism of type I dehydroquinase dehydratases from structures of reaction intermediates. *J. Biol. Chem.* **2011**, *286*, 3531–3539. [[CrossRef](#)]
16. Bradford, M.M. A Rapid and Sensitive Method for the Quantitation of Microgram Quantities of Protein Utilizing the Principle of Protein-Dye Binding. *Anal. Biochem.* **1976**, *72*, 248–254. [[CrossRef](#)]
17. Jaafar, N.R.; Mahadi, N.M.; Mackeen, M.M.; Ilias, R.M.; Murad, A.M.A.; Abu Bakar, F.D. Structural and functional characterisation of a cold-active yet heat-tolerant dehydroquinase from Glaciozyma antarctica PI12. *J. Biotechnol.* **2021**, *329*, 118–127. [[CrossRef](#)]
18. Sievers, F.; Wilm, A.; Dineen, D.; Gibson, T.J.; Karplus, K.; Li, W.; Lopez, R.; McWilliam, H.; Remmert, M.; Söding, J.; et al. Fast, scalable generation of high-quality protein multiple sequence alignments using Clustal Omega. *Mol. Syst. Biol.* **2011**, *7*, 539. [[CrossRef](#)]
19. Robert, X.; Gouet, P. Deciphering key features in protein structures with the new ENDscript server. *Nucleic Acids Res.* **2014**, *42*, W320–W324. [[CrossRef](#)]
20. Segel, H.I. *Enzyme Kinetics: Behavior and Analysis of Rapid Equilibrium and Steady-State Enzyme Systems*; Wiley: New York, NY, USA, 1993; pp. 18–80.
21. Avitia-Domínguez, C.; Sierra-Campos, E.; Salas-Pacheco, J.M.; Nájera, H.; Rojo-Domínguez, A.; Cisneros-Martínez, J.; Téllez-Valencia, A. Inhibition and biochemical characterization of methicillin-resistant staphylococcus aureus shikimate dehydrogenase: An in silico and kinetic study. *Molecules* **2014**, *19*, 4491–4509. [[CrossRef](#)]
22. Hernández-Alcántara, G.; Rodríguez-Romero, A.; Reyes-Vivas, H.; Peon, J.; Cabrera, N.; Ortiz, C.; Enríquez-Flores, S.; De la Mora-De la Mora, I.; López-Velázquez, G. Unraveling the mechanisms of tryptophan fluorescence quenching in the triosephosphate isomerase from Giardia lamblia. *Biochim. Biophys. Acta Proteins Proteom.* **2008**, *1784*, 1493–1500. [[CrossRef](#)]
23. Patel, A.; Shah, A. Purification and characterization of novel, thermostable and non-processive GH5 family endoglucanase from Fomitopsis meliae CFA 2. *Int. J. Biol. Macromol.* **2021**, *182*, 1161–1169. [[CrossRef](#)] [[PubMed](#)]
24. Yao, Y.; Li, Z.S. New insights into the mechanism of the Schiff base hydrolysis catalyzed by type I dehydroquinase dehydratase from S. enterica: A theoretical study. *Org. Biomol. Chem.* **2012**, *10*, 7037–7044. [[CrossRef](#)] [[PubMed](#)]
25. Liu, C.; Liu, Y.M.; Sun, Q.L.; Jiang, C.Y.; Liu, S.J. Unraveling the kinetic diversity of microbial 3-dehydroquinase dehydratases of shikimate pathway. *AMB Express.* **2015**, *5*, 7. [[CrossRef](#)] [[PubMed](#)]
26. Moore, J.D.; Hawkins, A.R.; Charles, I.G.; Deka, R.; Coggins, J.R.; Cooper, A.; Kelly, S.M.; Price, N.C. Characterization of the type I dehydroquinase from Salmonella typhi. *Biochem. J.* **1993**, *295*, 277–285. [[CrossRef](#)]
27. Light, S.H.; Antanasijevic, A.; Krishna, S.N.; Caffrey, M.; Anderson, W.F.; Lavie, A. Crystal structures of type I dehydroquinase dehydratase in complex with quinone and shikimate suggest a novel mechanism of schiff base formation. *Biochemistry* **2014**, *53*, 872–880. [[CrossRef](#)]
28. Mitsuhashi, S.; Davis, B.D. Conversion of 5-dehydroquinic acid to 5-dehydroshikimic acid by 5-dehydroquinase. *Biochim. Biophys. Acta* **1954**, *15*, 54–61. [[CrossRef](#)]
29. Adachi, O.; Ano, Y.; Toyama, H.; Matsushita, K. A novel 3-dehydroquinase dehydratase catalyzing extracellular formation of 3-dehydroshikimate by oxidative fermentation of Gluconobacter oxydans IFO 3244. *Biosci. Biotechnol. Biochem.* **2008**, *72*, 1475–1482. [[CrossRef](#)]
30. Kleanthous, C.; Reilly, M.; Cooper, A.; Kelly, S.; Price, N.C.; Coggins, D.J.R. Stabilization of the shikimate pathway enzyme dehydroquinase by covalently bound ligand. *J. Biol. Chem.* **1991**, *266*, 10893–10898. [[CrossRef](#)]
31. Salehi, M. Evaluating the industrial potential of naturally occurring proteases: A focus on kinetic and thermodynamic parameters. *Int. J. Biol. Macromol.* **2024**, *254*, 127782. [[CrossRef](#)]
32. Duman, Y.A.; Tekin, N. Kinetic and thermodynamic properties of purified alkaline protease from Bacillus pumilus Y7 and non-covalent immobilization to poly(vinylimidazole)/clay hydrogel. *Eng. Life Sci.* **2020**, *20*, 36–49. [[CrossRef](#)]
33. Aguilar, J.G.D.S.; de Castro, R.J.S.; Sato, H.H. Alkaline protease production by Bacillus licheniformis LBA 46 in a bench reactor: Effect of temperature and agitation. *Braz. J. Chem. Eng.* **2019**, *36*, 615–625. [[CrossRef](#)]
34. Steinweg, J.M.; Jagadamma, S.; Frerichs, J.; Mayes, M.A. Activation Energy of Extracellular Enzymes in Soils from Different Biomes. *PLoS ONE* **2013**, *8*, e59943. [[CrossRef](#)] [[PubMed](#)]
35. Souza, P.M.; Aliakbarian, B.; Filho, E.X.F.; Magalhães, P.O.; Junior, A.P.; Converti, A.; Perego, P. Kinetic and thermodynamic studies of a novel acid protease from Aspergillus foetidus. *Int. J. Biol. Macromol.* **2015**, *81*, 17–21. [[CrossRef](#)] [[PubMed](#)]

36. Ibrahim, E.; Mahmoud, A.; Jones, K.D.; Taylor, K.E.; Hosseney, E.N.; Mills, P.L.; Escudero, J.M. Kinetics and thermodynamics of thermal inactivation for recombinant *Escherichia coli* cellulases, cel12B, cel8C, and polygalacturonase, peh28; biocatalysts for biofuel precursor production. *J. Biochem.* **2021**, *169*, 109–117. [[CrossRef](#)] [[PubMed](#)]
37. Gouzi, H.; Depagne, C.; Coradin, T. Kinetics and thermodynamics of the thermal inactivation of polyphenol oxidase in an aqueous extract from *Agaricus bisporus*. *J. Agric. Food Chem.* **2012**, *60*, 500–506. [[CrossRef](#)]
38. Olusesan, A.T.; Azura, L.K.; Forghani, B.; Abu Bakar, F.; Mohamed, A.K.S.; Radu, S.; Manap, M.Y.A.; Saari, N. Purification, characterization and thermal inactivation kinetics of a non-regioselective thermostable lipase from a genotypically identified extremophilic *Bacillus subtilis* NS 8. *N. Biotechnol.* **2011**, *28*, 738–745. [[CrossRef](#)]
39. Batista, K.A.; Batista, G.L.A.; Alves, G.L.; Fernandes, K.F. Extraction, partial purification and characterization of polyphenol oxidase from *Solanum lycocarpum* fruits. *J. Mol. Catal. B Enzym.* **2014**, *102*, 211–217. [[CrossRef](#)]
40. González-Bello, C.; Tizón, L.; Lence, E.; Otero, J.M.; van Raaij, M.J.; Martínez-Guitián, M.; Beceiro, A.; Thompson, P.; Hawkins, A.R. Chemical Modification of a Dehydratase Enzyme Involved in Bacterial Virulence by an Ammonium Derivative: Evidence of its Active Site Covalent Adduct. *J. Am. Chem. Soc.* **2015**, *137*, 9333–9343. [[CrossRef](#)]
41. Lence, E.; Maneiro, M.; Sanz-Gaitero, M.; van Raaij, M.J.; Thompson, P.; Hawkins, A.R.; González-Bello, C. Self-Immolation of a Bacterial Dehydratase Enzyme by its Epoxide Product. *Chemistry* **2020**, *26*, 8035–8044. [[CrossRef](#)]
42. Millán-Pacheco, C.; Rios-Soto, L.; Corral-Rodríguez, N.; Sierra-Campos, E.; Valdez-Solana, M.; Téllez-Valencia, A.; Avitia-Domínguez, C. Discovery of Potential Noncovalent Inhibitors of Dehydroquinase Dehydratase from Methicillin-Resistant *Staphylococcus aureus* through Computational-Driven Drug Design. *Pharmaceuticals* **2023**, *16*, 1148. [[CrossRef](#)]

Disclaimer/Publisher's Note: The statements, opinions and data contained in all publications are solely those of the individual author(s) and contributor(s) and not of MDPI and/or the editor(s). MDPI and/or the editor(s) disclaim responsibility for any injury to people or property resulting from any ideas, methods, instructions or products referred to in the content.